

Improving High-Temperature Strength of Ti-6Al-2.5Mo-1.5Cr-0.5Fe-0.3Si Titanium Alloy by Cryogenic Pre-treatment and Laser Peening



JIE SHENG, SHU HUANG, MUXI LIU, and FENGZE DAI

The plastic deformation behavior and microscopic strengthening mechanism of Ti-6Al-2.5Mo-1.5Cr-0.5Fe-0.3Si (TC6) titanium alloy treated by the combination of cryogenic pre-treatment (CT) and laser peening (LP) during a high-temperature tensile testing were investigated. The residual stress and full-width-half-maximum (FWHM) values were determined by X-ray diffraction. In addition, micro-structural evolution in the subsurface was characterized by optical microscopy (OM) and transmission electron microscopy (TEM). It was found that the yield strength of CT-LP samples was 14.09, 29.46, and 23.37 pct higher than that of the LP samples at 400 °C, 500 °C, and 600 °C, respectively, due to less thermal relaxation of compressive residual stress (CRS) and more refined grains. Furthermore, widely distributed dislocation walls and tangled dislocations in CT-LP samples verified the strengthening effects induced by the combination of CT and LP. A novel “paw-shaped” structure which was adhered stably on the grain boundaries was a direct evidence of the strengthening effects. The unmovable dislocation jogs generated by multi-direction dislocation movement and the cross-slip structure were believed to be two important factors to improve the high-temperature strength of TC6 titanium alloy.

<https://doi.org/10.1007/s11661-020-05789-y>

© The Minerals, Metals & Materials Society and ASM International 2020

I. INTRODUCTION

NOWADAYS, Ti-6Al-2.5Mo-1.5Cr-0.5Fe-0.3Si (TC6) titanium alloy is widely used to manufacture key components of aerospace engines and compressors due to its high mechanical strength, excellent corrosion, and oxidation resistance.^[1,2] However, while serve in severe conditions such as extreme temperature and ultimate load, the mechanical properties of TC6 titanium alloy will decline. In particular, high temperature results in creep and oxidation effect, significantly decreasing the performance of TC6 titanium alloy. Therefore, it is of necessity to enhance the surface properties of titanium alloy at high temperature.^[3]

Recently, various surface deformation strengthening technologies, such as deep rolling,^[4] cavitation peening,^[5] shot peening,^[6] and laser peening^[7,8] (LP), have been utilized to enhance the properties of titanium alloy. Compared with other surface treatment technologies, LP process could induce much higher compressive residual stress (CRS) with deeper effect, as well as more

refined grains, to improve the mechanical properties of alloys.^[9–13] What is more, LP is a non-contact treatment that avoids damaging the alloy surface. Therefore, LP has been recognized as an effective method to enhance fatigue life and resistance to wear and hydrogen embrittlement at room temperature.^[14–17] However, some scholars have found that high-level CRS induced by LP was relaxed under high temperature.^[18] In addition, the crystal defects (*e.g.*, dislocations) induced by LP were rearranged and annihilated, while the refined grains in the superficial layer were grown under high temperature,^[3,19] eventually weakening the strengthening effect of LP.

Cryogenic treatment^[20] (CT) is executed by placing alloys in an ultra-low temperature to improve their mechanical and physical properties. It has been reported that considerable dislocations and sub-grains induced by volume shrinkage effects of CT led to stable microstructures. With the accumulation of the dislocation motion, dislocation tangling obviously occurs and delays the initiation of fatigue crack.^[21] Meanwhile, CT can greatly affect the residual stress distribution^[22] and tensile properties.^[23] In order to improve the stability of microstructures and residual stress induced by LP at high temperature, a compound technique combined with CT and LP has been proposed.

So far, several reports about CT-LP are available in the literature. For instance, Ye *et al.*^[24] investigated the

JIE SHENG, SHU HUANG, MUXI LIU, and FENGZE DAI are with the School of Mechanical and Engineering, Jiangsu University, Zhenjiang 212013, China. Contact e-mail: huangshu11@sina.com

Manuscript submitted November 15, 2019.

Article published online April 30, 2020

microstructure and mechanical properties of copper subjected to cryogenic laser peening (CLP). It was found that CLP could provide higher material strength with better thermal stability. Li *et al.*^[25] illustrated that CT-LP produced more precipitated second phases, higher density of dislocation and CRS. Beneficial micro-structural evolution and CRS induced by CT-LP were considered to be the main factors that contributed to the improvement of fatigue properties on 2024-T351 aluminum alloy.

During the process of CT-LP, volume shrinkage effect induced by CT combined with laser shock waves effect induced by LP could generate mixed plastic deformation layer on the surface of treated material. However, the superimposed effects of CT-LP on the plastic deformation behavior and micro-strengthening mechanism of TC6 titanium alloy are still pending. The previous experiments from our group exhibited that CT prior to LP could induce finer grains and higher dislocation density in TC6 alloy, resulting in better mechanical properties, when comparing to single CT or LP process.^[26] We subsequently used a tensile test to verify that the strengthening effect of CT-LP was still working even under higher temperature.^[19] It was initially concluded that more beneficial microstructures, like deformation twins, and high density of dislocations introduced by CT-LP play a critical role in improving the mechanical properties of TC6 titanium alloy. However, the interactions effects of ultra-low temperature (CT) and ultra-high strain rate (LP) on micro-structural evolution at high temperature is still unclear. More typical microstructures and direct evidences for improving high-temperature stability are required to further verify our viewpoint.

In this study, we carried out a complete set of experiments to investigate the influences of CT-LP on mechanical properties and micro-structural evolution of TC6 titanium alloy at high temperature. The detailed strengthening mechanism induced by CT-LP technique is discussed from both macro- and micro-sides. The research on high-temperature plastic deformation behavior and microscopic strengthening mechanism of TC6 titanium alloy subjected to CT-LP is of practical value in industry application.

II. EXPERIMENTS AND METHODS

A. Materials

The chemical composition and mechanical properties of TC6 titanium alloy used in this study are given in Tables I and II, respectively. TC6 titanium alloy is primarily composed of the hexagonal close-packed α (brighter regions) phase and the body-centered cubic β (darker regions) phase, the β phases evenly disperse in the boundaries of equiaxed α grains. Rectangular samples (Figure 1(b)) with dimensions of 35 mm \times 15 mm \times 5 mm (length \times width \times thickness) and tensile samples (Figure 1(a)) were cut from a TC6 titanium alloy plate with the thickness of 5 mm by electron

discharge machining (EDM). In detail, samples with geometry and dimensions are illustrated in Figure 1. Prior to the experiment, the surfaces of the samples were sanded by SiC papers with different grades of roughness from 600# to 2000#, and then polished by grinding paste on abrasive finishing machine until mirror-shaped surfaces were obtained. Finally, the samples were preserved in a drying box after ethanol ultrasonic cleaning to make sure the residual stress caused by cutting and polishing reached its minimum amplitude value.

B. Experimental Processes

A well-insulated incubator filled with liquid nitrogen was used to provide a cryogenic environment for the CT samples, for which the temperature was kept at 77 K and the soaking time of polished samples was 12 hours. After CT, the samples were taken out from the incubator and recovered to room temperature. LP experiments were subsequently performed at room temperature by using a Q-switched GAIA Nd:YAG laser system (as shown in Figure 2) with the parameters listed in Table III. The footprint of laser spot with a diameter of 3 mm was hat-top, and the overlapping rate between the adjacent spots was 50 pct, as shown in Figures 1(b) and (c). Additionally, 3M professional aluminum tape with a thickness of 120 μ m was selected as an ablation medium for plasma initiation to protect the samples surface from thermal damage, and flowing water with a thickness of about 1 mm was used as the plasma confinement layer. Double-side LP was adopted for all the samples.

Furthermore, thermal exposure tests were performed to investigate micro-structural evolution and residual stress relaxation of LPed and CT-LPed samples at high temperature. In detail, the samples were exposed at high temperatures of 400 $^{\circ}$ C, 500 $^{\circ}$ C, and 600 $^{\circ}$ C in a vacuum furnace for 50, 100, 150, 200, 250, and 300 minutes, respectively. Then, the samples were air cooled to room temperature naturally.

C. Measurement of Residual Stress

Prior to the measurement of surface residual stress, the samples were cleaned manually by ethanol to remove the sticky aluminum foil produced during LP. A type of X-350A X-ray diffraction system was used in this study. All measurement of residual stress and full-width-half-maximum (FWHM) value was determined on the top surface of samples by X-ray diffraction with $\sin^2\psi$ method. The tilts angles were 0, 25, 35, and 45 deg, respectively. The scanning starting and terminating angles were 146 and 136 deg, respectively. The feed angle of the ladder scanning was 0.1 deg s^{-1} . An X-ray tube with a chrome anode operated at 22 kV was used. $CuK\alpha$ ray was selected as X-ray source. The diameter of collimator was Φ 1 mm. Three points which marked in Figure 1(b) of each sample were measured, and the average value was taken as the final residual stress result.

Table I. Composition of TC6 Titanium Alloy

Element	Al	Mo	Cr	Fe	Si	C	N	H	O	Ti
Wt Pct	5.5–7.0	2.0–3.0	0.8–2.3	0.2–0.7	0.15–0.40	0.10	0.05	0.015	0.18	bal.

Table II. Mechanical Properties of TC6 Titanium Alloy at Room Temperature

Properties	Yield Strength (MPa)	Tensile Strength (MPa)	Young Modulus (GPa)	Elongation to Rupture (Pct)
Values	885	980	110	12.6

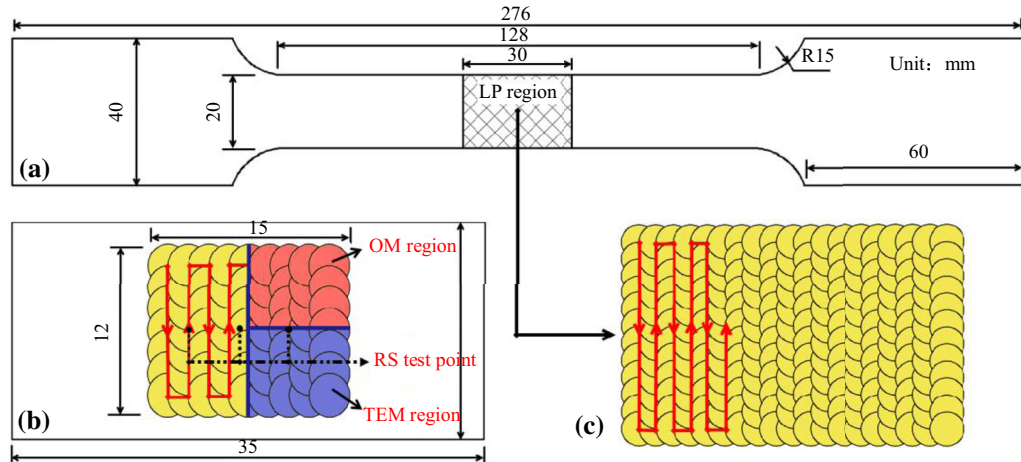


Fig. 1—Geometry and dimensions of (a) tensile sample and (b) rectangular sample; (c) LP path of tensile sample.

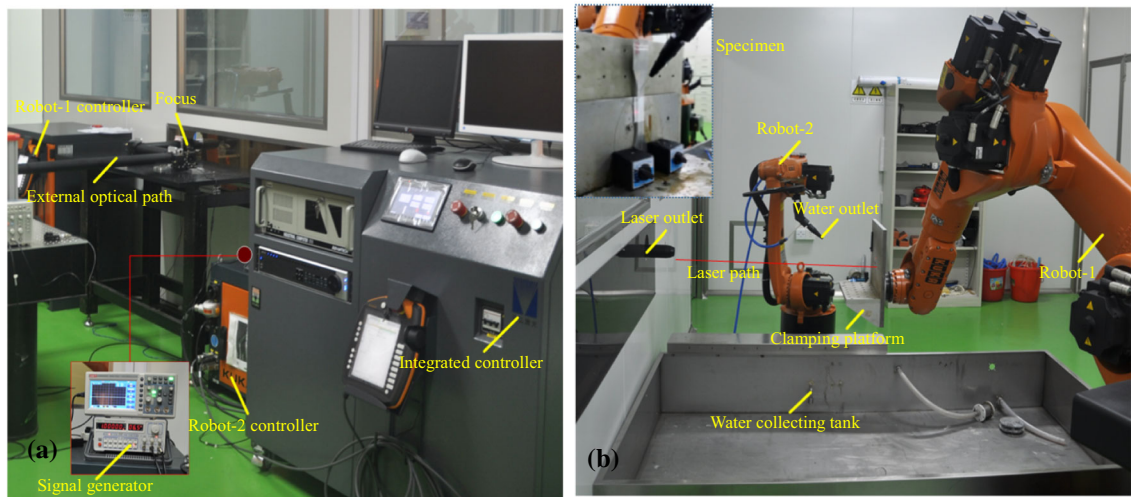


Fig. 2—Robots and the cooperative control system with laser (a) control system and (b) robots.

D. High-Temperature Tensile Tests and Fracture Observation

Tensile tests were conducted on an MTS 809 servo-hydraulic material testing system with 2 mm/min tensile rate at different temperatures of 400 °C, 500 °C, and 600 °C, respectively. The size of dog-bone tensile

samples and LP path is shown in Figures 1(a) and (c). To minimize thermal gradients and keep the temperature error within ± 2 °C, the samples were pre-heated by an electrical resistance furnace (RX3-50-13) for 10 minutes. After high-temperature tensile test, the tensile fracture surfaces were ethanol ultrasonic cleaned for 15

minutes to remove oil and other impurities. Then fracture morphologies of tensile fracture were observed by using an S-3400N SEM. An EDS test was performed to determine the typical structures in the tensile fracture.

E. Microstructure Observation

After thermal exposure test, samples treated by LP and CT-LP were cut into square shape sizes of 10 mm × 10 mm × 5 mm by using an electrical discharge machine (EDM) to perform a microstructure through thickness. The samples were sanded by SiC papers with different grades of roughness from 600# to 2000#, and then polished by grinding paste on abrasive finishing machine until mirror-shaped surfaces are obtained. A corrosive liquid solution consisting of 4 vol pct HF, 10 vol pct HNO₃, and 86 vol pct H₂O was used to etch samples for 15 seconds. Then, optical microscopy was used to observe the grain evolution of LPed and CT-LPed samples. The test points of OM specimen is shown in Figure 1(b).

In order to further analyze micro-structural evolution during thermal exposure test, the microstructure in the subsurface layer of LPed and CT-LPed samples was characterized by a JEM-2100 TEM operated at a voltage of 200 kV. Thin foils at a depth of 30 and 80 μm from top surface were prepared. In detail, the top surface of samples was polished to the given depth and then cut off into several pieces parallel to surface. The thin foils were polished to the thickness of 50 μm. Finally, electropolishing device was used to ion-thin the foils. To well present the detailed experiment process, a schema is exhibited as Figure 3.

III. RESULTS AND DISCUSSION

A. Residual Stress Analysis

The surface CRSes of LPed and CT-LPed TC6 samples after thermal exposure test are presented in Figure 4. It is noted that CRS of CT-LPed sample is around – 628 MPa at room temperature. This value is larger than that of LPed sample with a value of – 565 MPa. The variation in value is attributed to two reasons. Firstly, as serves in the ultra-low temperature, the different expansion coefficients of phases and grains of TC6 alloys lead to a non-uniform volume shrinkage, which introduces internal CRSes after the recovery process of CT.^[25–27] Secondly, the subsequent LP process generates severe plastic deformation by instantaneous laser shock wave, and thus induces high-amplitude surface CRSes. The two generated stresses mentioned above are superimposed to enhance the surface CRSes of the CT-LPed samples.

However, the induced CRSes tend to relax at high temperature.^[28,29] From Figure 4, it is clear that CRS of LPed sample is relaxed by 5.13 pct, while this value of CT-LPed sample is 4.78 pct after a thermal exposure at 400 °C for 100 minutes. Further, the relaxation rate increases with an increase in temperature. For instance, after been exposed at 600 °C for 100 minutes, the CRSes

of LPed and CT-LPed samples are relaxed by 58.94 and 48.09 pct, respectively, which are much higher than that at 400 °C. Moreover, it is noteworthy that CRS relaxes drastically in the first 100 minutes, and then decays to constant level. For example, the CRS of CT-LPed sample is relaxed by 48.09 pct at 600 °C in the first 100 minutes, and then relaxed by 25.77 and 9.92 pct from 100 to 200 minutes and from 200 to 300 minutes, respectively. This conclusion is well consistent with Kattoura's report.^[30]

To sum up, the CRS relaxation rate of both LPed and CT-LPed samples increases with an increase in exposure temperature and time. Compared with LP, CRS induced by CT-LP is more stable and still superior. For instance, CRSes of CT-LPed samples are 11.57, 27.54, and 40.52 pct higher than that of LPed samples at 400 °C, 500 °C, and 600 °C for 100 minutes, respectively. We can infer that the thermally activated dislocations slip in the thermal recovery process plays important role during the relaxation period.^[18,31] As a result, CT-LP-induced CRS exhibits better high-temperature stability as compared to LP treatment.

B. Full-Width-Half-Maximum

Full-width-half-maximum (FWHM) graphical representation of the LPed and CT-LPed TC6 samples is shown in Figure 5. Note that FWHM values of LPed TC6 samples are decreased by 0.85, 1.69, and 2.12 pct after been exposed at 400 °C for 100, 200, and 300 minutes. As comparison, the FWHM values of CT-LPed samples are decreased by 0.41, 1.65, and 2.06 pct, respectively. Normally, the FWHM value is used to quantify the dislocation density of alloys.^[32,33] Therefore, it is evident that the CT-LP treatment alleviates the annihilation of dislocations in the TC6 alloy at high temperature as compared to LP. In addition, it appears from Figure 5 that the FWHM values of CT-LPed samples are 2.38, 2.34, and 2.21 after been exposed at 400 °C, 500 °C, and 600 °C, respectively. The pronounced negative relation between FWHM values and temperatures illustrates that the dislocation density decreases with an increase in temperature, which further confirms the conclusion of surface CRS relaxation in Section III-A.

It is well known that atomic diffusion causes a recovery effect, followed by proliferation and migration of dislocation at elevated temperature.^[34] Further, the atomic chattering as well as diffusion motion are both intensified with the increase of exposure temperature.^[35] High distortion lattice accelerates atoms moving to equilibrium positions, and thus weakens the lattice distortion. While atoms and vacancies migrate on a large scale, the dislocation mobility also increases, thereby increasing the trap of dislocation annihilation and weakening the obstacle of dislocation movement.^[31] As a result, a large number of dislocations induced by LP and CT-LP on the superficial layer shift from high energy state to low energy state, consequently releasing the dislocation entanglement. This process is recognized as the root cause of CRS relaxation of TC6 samples. However, when compared with LP, CT-LPed technique

Table III. Parameters of Q-Switched GAIA Nd:YAG Laser System

Parameters	Laser Wavelength (nm)	Pulse Duration (ns)	Laser Energy (J)	Laser Power Density [(GW/cm ²)]	Repetition Rate (Hz)
Value	1064	10	9	11.46	5

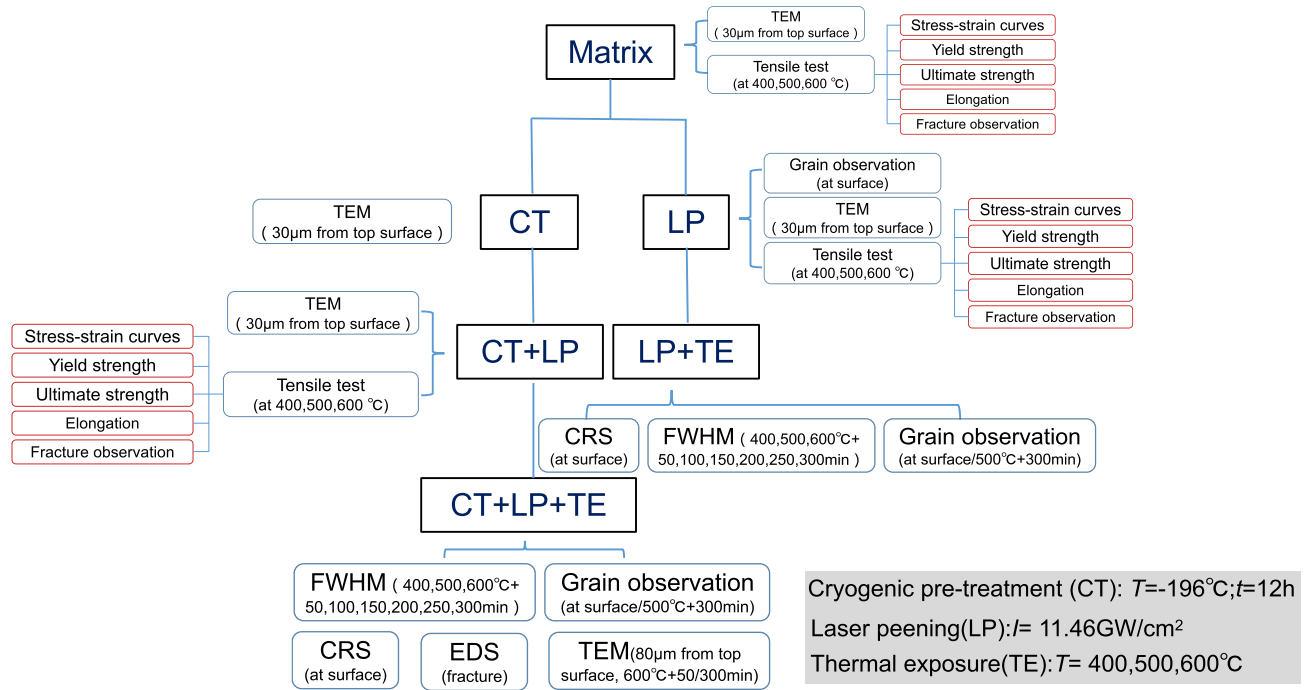


Fig. 3—Schema of experimental process.

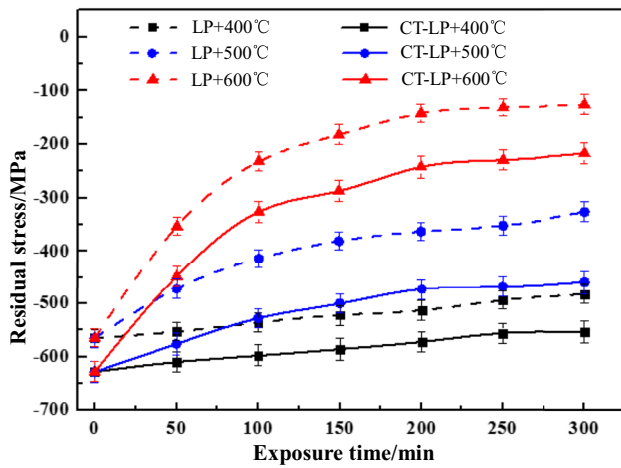


Fig. 4—Residual stresses of LPed and CT-LPed TC6 samples after thermal exposure test.

produces both considerable dislocations induced by volume shrinkage effects of CT and high density of entangled dislocations caused by LP. These superimposed dislocations make it harder to annihilate at high temperature, and correspond to stable high-temperature properties.

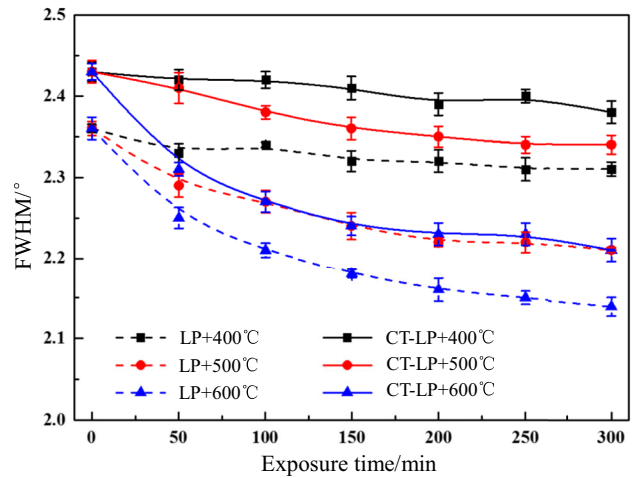


Fig. 5—FWHM values of LPed and CT-LPed TC6 samples after thermal exposure test.

C. Microstructure Observation

1. Grain evolution

In order to investigate the grain evolution behavior of LPed and CT-LPed samples during thermal exposure process, grain morphologies were observed by OM, as

shown in Figure 6. Note that the α phases and β phases are fully distributed in the TC6 alloy. Compared with original grains, pronounced grain refinement is found in both LPed and CT-LPed samples, as shown in Figures 6(a) and (b). Due to the dislocation proliferation caused by LP and CT-LP, high density of dislocations is moved and tangled inside the grains, slowly forming the so-called dislocation walls. These dislocation walls and sub-dislocation walls re-divide the grains into smaller scales, which results in the grain refinement.^[36,37]

However, both refined grains growth quickly at high temperature, as shown in Figures 6(c) and (d). This is due to the fact that high temperature improves the diffusion of atoms, which accelerates the movement of grain boundaries, and eventually results in the increment of grain size. Additionally, the diffusion capacity of α phase boundary is increased at high temperature. As a result, the fine α phases are swallowed, leading to an increase in grain size. Even so, the increment in grain size of CT-LPed samples is less pronounced as compared to that of LPed samples while exposed at 500 °C for 300 minutes. This evidence is well consistent with the conclusion in Section III-A.

2. Microstructure evolution of CT-LPed samples at high temperature

To further analyze the micro-structural characteristics, dislocation structures at a depth of 30 and 80 μm from the top surface of CL-LPed TC6 samples after different thermal exposure tests are exhibited. Figure 7 represents the TEM morphologies of dislocation structures in matrix, CT, LPed, and CT-LPed samples, respectively. In detail, Figure 7(a) shows that internal grain boundary is clear in matrix material, and very few dislocation lines and dislocation tangles exist inside the grains. After CT, some dislocation tangles and slip bands are exhibited in the single grain of TC6 alloy, as shown in Figure 7(b), which is attributed to the plastic deformation caused by a sharp volume shrinkage. During CT process, the unidirectional shear slip bands are generated inside the grains when the extrusion stress exceeds the shear ultimate strength of the grains. However, the slip bands do not cross the grain boundaries but have been terminated at the grain boundaries. The strong binding force of grain boundary atoms and the tangled dislocations strengthen the grain boundaries, which ultimately make it hard to puncture.

Figure 7(c) shows that multitude dislocation structures such as dislocation lines and dislocation cells are

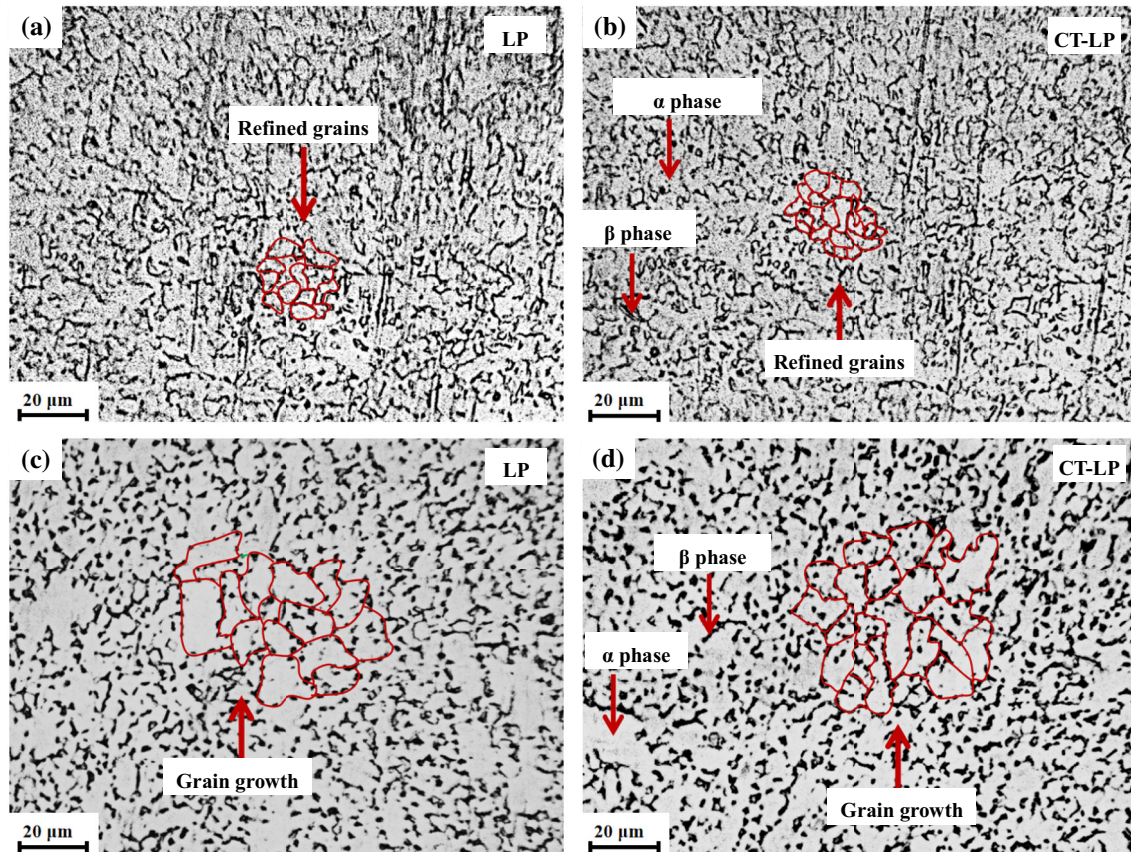


Fig. 6—Grain morphologies of (a) LPed sample; (b) CT-LPed sample; (c) LPed sample exposed at 500 °C for 300 min; (d) CT-LPed sample exposed at 500 °C for 300 min.

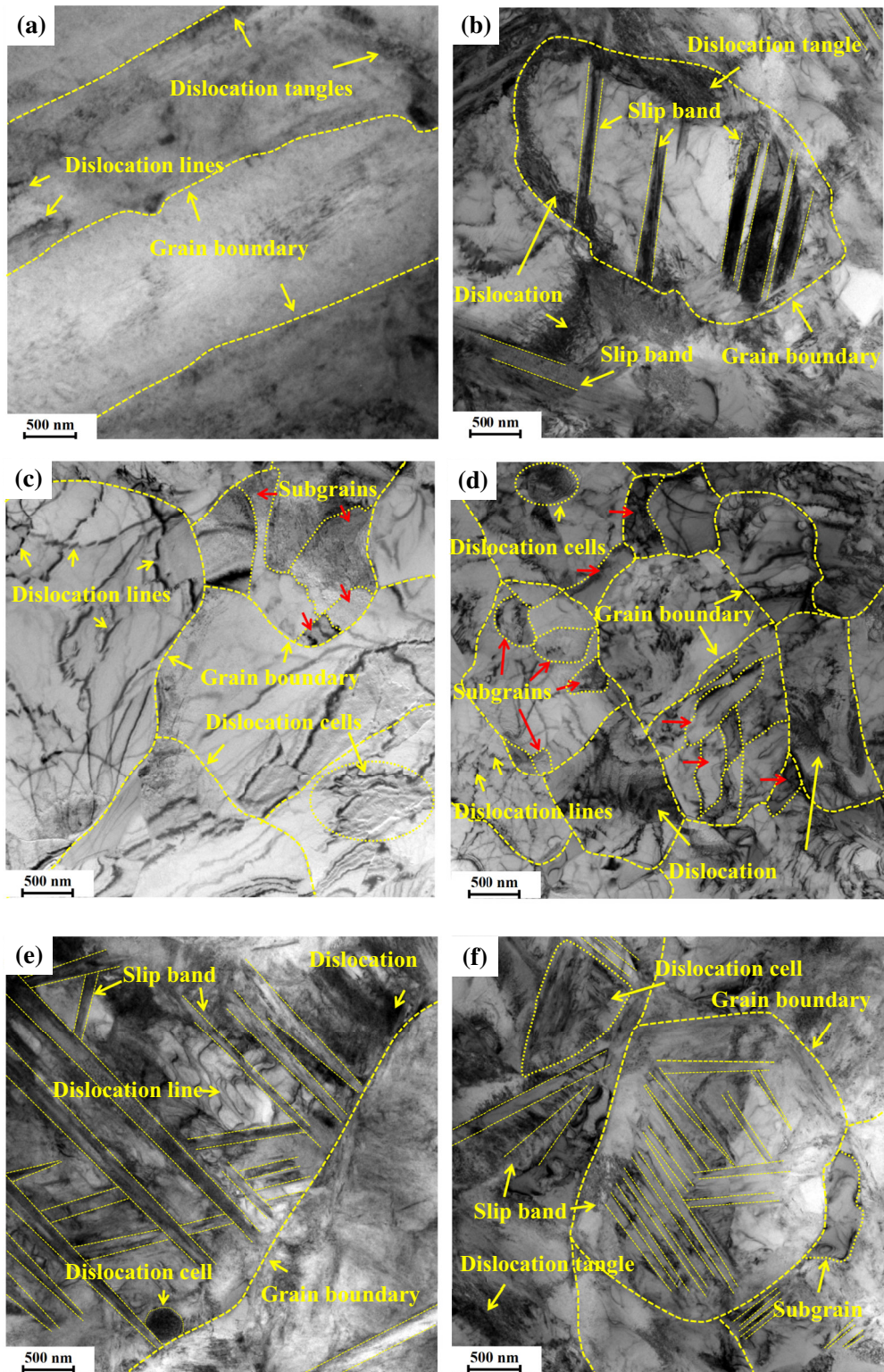


Fig. 7—TEM images of microstructures at a depth of 30 μm from the top surface of TC6 samples at room temperature: (a) matrix, (b) CT, (c) LPed, and (d) CT-LPed samples, (e) slip bands around grain boundary, and (f) slip bands inside grains of CT-LPed samples.

generated due to severe plastic deformation caused by LP. Further, some sub-grains are also observed. Compared with CTed samples, more dislocation structures such as dislocation lines, dislocation tangles, and dislocation cells are found widely distributed in the CT-LPed

samples, as shown in Figure 7(d). Also, it is worth noting that more sub-grains are generated near the grain boundary. Two facts are considered as the reasons for this evolution. Firstly, CT process significantly suppresses the dynamic response of dislocation and inhibits

its sliding and annihilation, which results in a higher density of dislocation structure. Secondly, LP treatment induces severe plastic deformation and generates large amount of dislocation-cell structures, higher density of dislocation, and tangled dislocations in the near-surface layer.

Theoretically, the interaction force τ_d between dislocations can be defined as^[38]

$$\tau_d = \alpha G b \rho^{1/2}, \quad [1]$$

where α is a proportional constant, G is the shear modulus, b is the vector length of dislocation, and ρ is the dislocation density. Eq. [1] indicates that the interaction force between dislocations increases with an increase in dislocation density. Higher density of dislocations induced by CT-LP contributes to higher interaction force between dislocations, finally enhancing the stability of strengthening microstructure at high temperature.

Slip bands are another important factor to strengthen the CT-LPed TC6 alloy. In Figures 7(e) and (f), a large number of slip bands are observed around the grain boundaries and inside the grains. These slip bands are supposed to be generated by the interaction of shock wave pressure and extrusion stress induced by volume shrinkage effects. Most of these slip bands are formed inside the grains, intersect together, but terminate at the grain boundaries. These microscopic characteristics further tangle the dislocations, making the strengthening structures much more stable than that of LPed samples.

It is well known that the interactions between dislocations induced by slip can generate jogs, which are not on slip plane. Generally, if the slip direction is inconsistent with the original slip direction, the jogs are then produced.^[39] It is interesting that typical dislocation jogs are observed on the micro-graph at a depth of 80 μm from the top surface of CT-LPed sample after being exposed at 500 $^{\circ}\text{C}$, as shown in Figures 8(a) and (b). In fact, there exist two kinds of slip process in CT-LP process: slips induced by volume shrinkage effect during CT process and slips induced by shock pressure during LP, as shown in Figures 8(c) through (e). Since the slip direction generated by LP is inconsistent with the slip direction induced by CT process, jogs are generated as obstacles for dislocation movement. Specially, unmovable jogs can aggravate dislocation tangle and eventually improve the stability of microstructure at high temperature.

TEM images of typical microstructure at a depth of 80 μm from the top surface of CT-LPed samples after being exposed at 600 $^{\circ}\text{C}$ for 50 and 300 minutes are presented in Figures 9(a) and (b), respectively. As the temperature and exposure time increase, atomic motion is more active and second phase particles are easy to precipitate, which tangled with the free-moving dislocations. The tangled dislocations are the original positions of the newly generated dislocation walls, which divide the large grains into small scale as can be seen in Figure 9(b). It is noted that even at 600 $^{\circ}\text{C}$, the newly generated dislocation walls are self-tangled, forming a “paw-shaped” structure, and was adhered on the grain

boundaries. This new structure could be a direct evidence for the strengthening effect of CT-LP process at high temperature.

D. Mechanical Properties

Figure 10 and Table IV present the comparing results of yield strength, ultimate strength, and elongation of LPed and CT-LPed samples at different temperatures. In Figure 10(a), the yield strength of CT-LPed samples are 862.18 MPa, 877.29 MPa, and 619.40 MPa at 400 $^{\circ}\text{C}$, 500 $^{\circ}\text{C}$, and 600 $^{\circ}\text{C}$, which are 14.09, 29.46, and 23.37 pct higher than that of the LPed samples, respectively. Similarly, in Figure 10(b), the ultimate strength of CT-LPed samples are 896.42 MPa, 913.25 MPa, and 654.73 MPa at 400 $^{\circ}\text{C}$, 500 $^{\circ}\text{C}$, and 600 $^{\circ}\text{C}$, which are 14.15, 27.49, and 27.92 pct higher than that of LPed samples, respectively. However, there is a slight loss in the plasticity of CT-LPed samples, decreased by only 2.14, 2.81, and 2.68 pct as compared to the LPed samples at 400 $^{\circ}\text{C}$, 500 $^{\circ}\text{C}$, and 600 $^{\circ}\text{C}$, respectively, as shown in Figure 10(c). It implies that CT-LP only sacrifices very little plasticity while obtaining substantial enhancement on the yield and ultimate strength of TC6 titanium alloy than LP.

The large improvement on the yield and ultimate strength after CT-LPed observed in Figure 10 is explained as follows. Theoretically, strength of a material can be calculated by adding contributions from the decrease in grain size (grain boundary strengthening) and increase in dislocation density (work hardening) with plastic deformation^[40,41]

$$\sigma_f = \sigma_0 + k(d_{fp})^{-1/2} + \alpha G b \rho^{1/2}, \quad [2]$$

where σ_f is the strength, σ_0 is a friction stress, k is the Hall–Petch constant, d_{fp} is the mean free path for dislocations, α is a constant, G is the shear modulus, b is the Burgers vector, and ρ is the dislocation density. From Eq. [2], it is deduced that the mean free path for dislocations and dislocation density have negative and positive contributions to the material strength, respectively. Therefore, higher density of dislocations produced by CT-LP treatment could induce higher material strength increment as well as higher stability at elevated temperature.

In addition, it is found that the yield strength of TC6 samples decreases with an increase in temperature from Figure 10. The phenomenon is due to the effect of softening mechanism at high temperature. High-temperature softening mechanism is explained by the interaction of solute atoms with mobile dislocations. During tensile deformation process, solute atoms diffuse into the dislocations and limit the movement of dislocations. As the temperature rises, the diffused solute atoms and dislocations form a movable “Koch” mass that reduces the yield stress.^[42] In summary, both LP and CT-LP can enhance yield strength, ultimate strength, as well as elongation of TC6 matrix material at high temperature. Furthermore, although there is a slight loss in plasticity, CT-LP exhibits better strengthening effects than single LP.

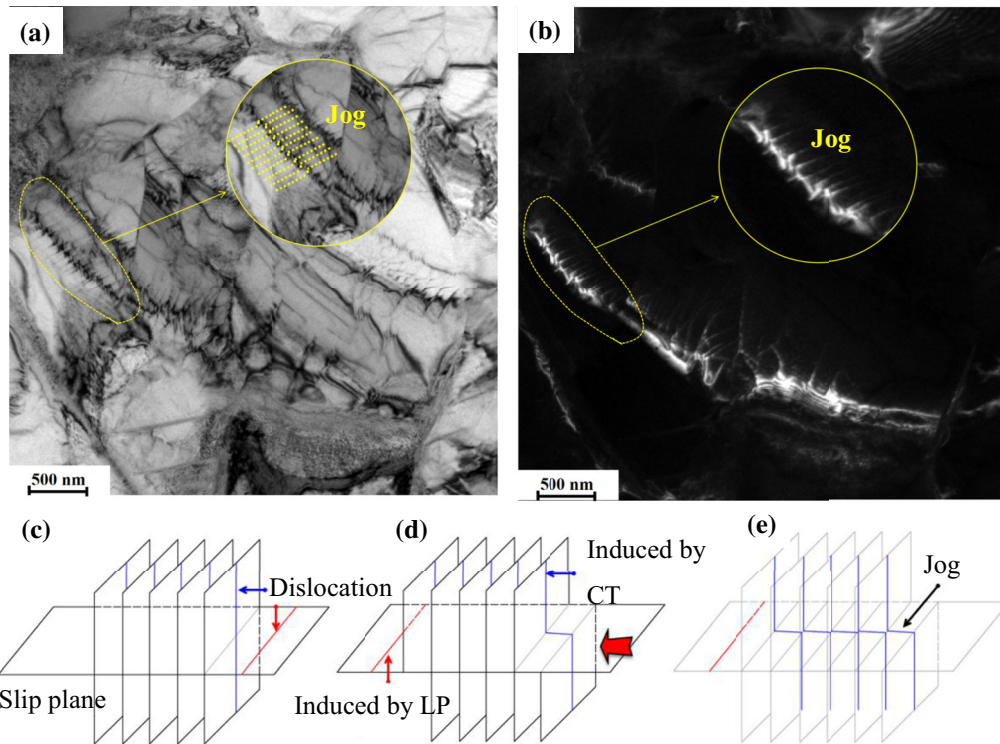


Fig. 8—TEM images of (a) bright-field, (b) dark-field of CT-LPed TC6 samples exposed at 500 °C as well as jog generation process of (c) before dislocation delivery, (d) after dislocation delivery, and (e) final status.

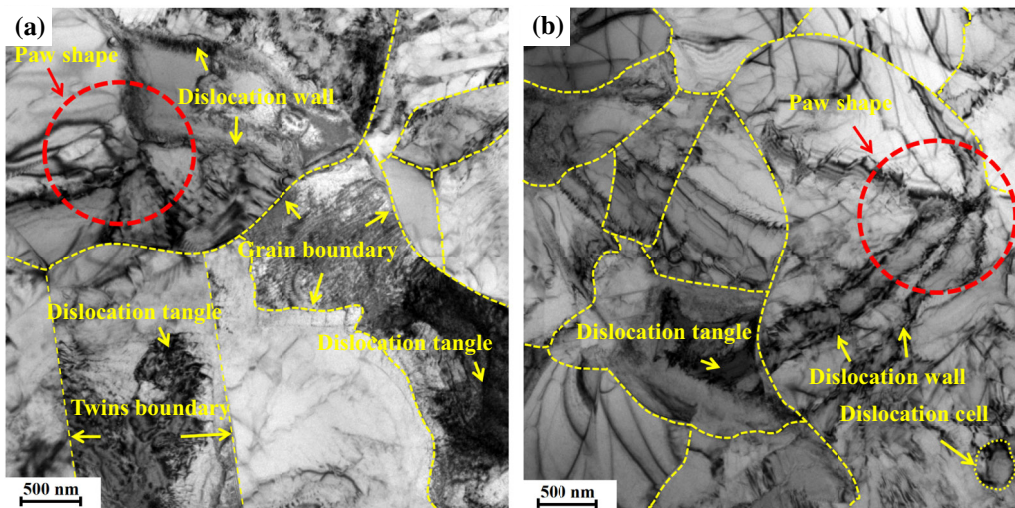


Fig. 9—TEM images of typical dislocation structure at a depth of 80 μm from the top surface of CT-LPed TC6 sample after being exposed at 600 °C for (a) 50 min and (b) 300 min.

E. Tensile Fracture Analysis

The fracture morphologies of TC6 samples were analyzed after high-temperature tensile tests, as shown in Figure 11. It is found that the samples treated by LP and CT-LP mainly present dimple fracture morphology and plastic fracture mode at high temperature. It appears from Figures 11(a) and (b) that the dimple size slightly decreases after CT-LP as compared with LP. This indicates a slight loss of plasticity for CT-LPed

samples, which is consistent with the result of elongation decrease in Figure 10. A similar trend is revealed for TC6 samples at 600 °C in Figures 11(e) and (f). It is worth noting that quasi-cleavage plane appears at the fracture surface of both samples at 500 °C, as shown in Figures 11(c) and (d). This implies that strengthening phases precipitated from TC6 alloy at 500 °C are involved in deformation and shearing during the high-temperature tensile. Compared with LP, the

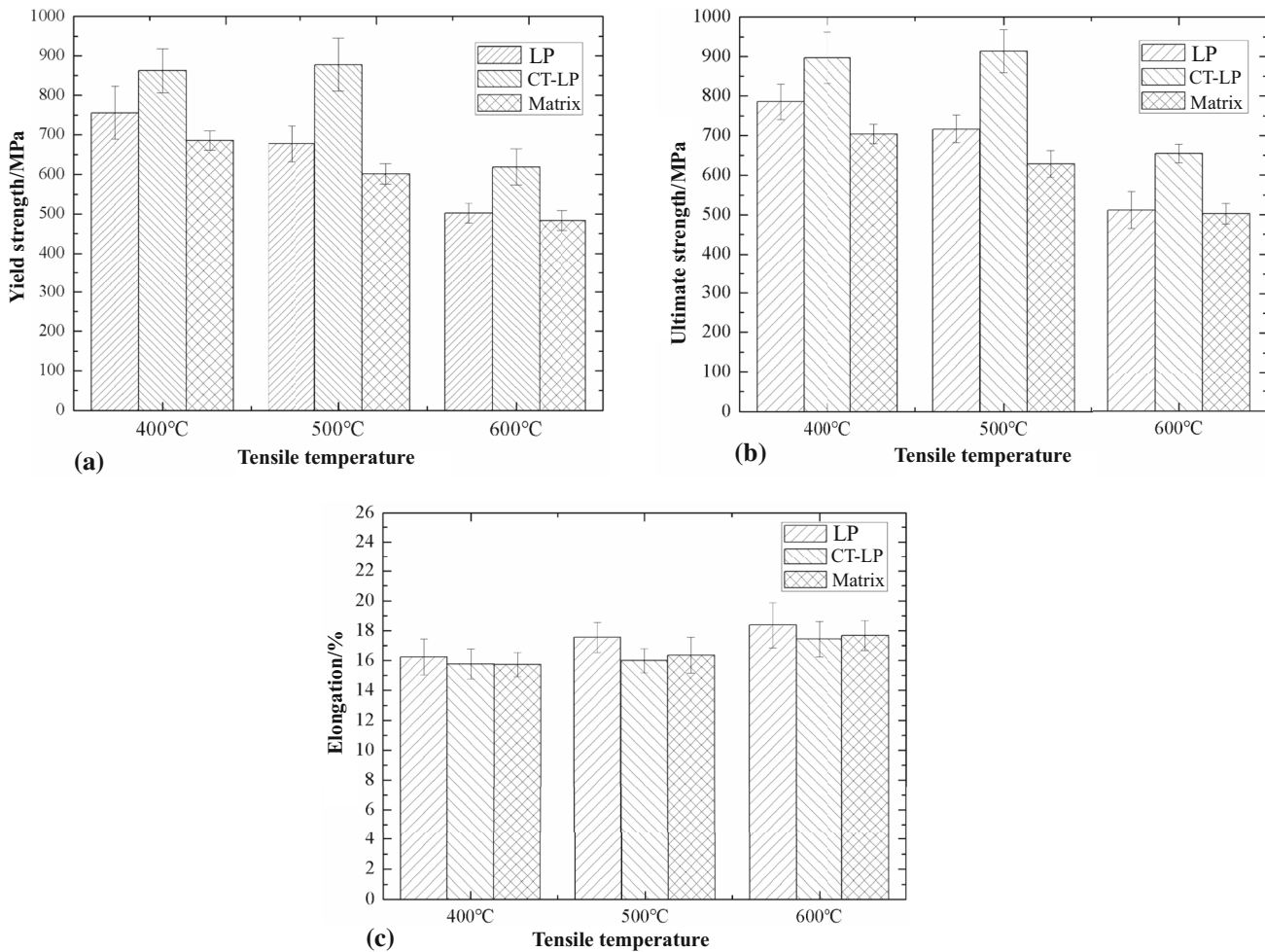


Fig. 10—Mechanical properties of LPed and CT-LPed samples at different temperatures: (a) yield strength, (b) ultimate strength, and (c) elongation.

quasi-cleavage planes caused by strengthening phases are larger on the fracture surface of CT-LPed samples, which verifies the plasticity drop. Comparing Figures 11(c) and (d), larger quasi-cleavage planes are found in the fracture of CT-LPed samples as compared to that of LPed samples at 500 °C. This phenomenon indicates that the CT-LPed samples could precipitate more uniformly distributed reinforcing phases and achieve better dispersion strengthening effect.

F. Strengthening Mechanism of CT-LP

Combined with the typical microscopic features, a schematic illustration of microscopic strengthening mechanism on CT-LPed TC6 titanium alloy is established, as shown in Figure 12.

Firstly, Figure 12(a) shows that CT induces a sharp volume shrinkage on the entire material. As a result, a multitude of dislocation is generated inside the original grains by plastic deformation. Since single grain is compressed by the surrounding material, the unidirectional shear slip bands are generated inside the grains when the extrusion stress exceeds the shear ultimate strength of the grains. However, the slip bands extend

inside the grain boundaries but terminate at the grain boundaries, as illustrated in Figure 7(b). The strong binding force of grain boundary atoms and tangled dislocations strengthen the grain boundaries and make it hard to puncture. In addition, ultra-low temperature of CT process can effectively restrain the dynamic response of dislocation as well as inhibit its annihilation, leading the lattice to accommodate higher density of dislocation structure.

Secondly, the CTed samples are subjected to LP treatment. Higher strain rates and severe plastic deformation induced by LP are believed to be conducive to generate slip bands, as shown in Figure 12(b). Since the slip direction generated by LP is inconsistent with that of CT process, the newly generated slip bands pass through the original slip bands and intersect with each other, as shown in Figure 12(c). The intersected slip bands around the grain boundaries and inside the grains are clearly seen in Figures 7(e) and (f). It indicates that the slip bands are crucial in the grain refinement of two-phase titanium alloy during severe plastic deformation.^[43] The cross-slip zone forms on the top surface after CT-LP treatment, effectively inhibits the grain growth, and then delays the movement of dislocation at

Table IV. Mechanical Properties of Matrix, CT-LP, and LP Samples at Different Temperatures

Parameters	Matrix			CT-LP			LP		
	400 °C	500 °C	600 °C	400 °C	500 °C	600 °C	400 °C	500 °C	600 °C
Yield Strength (MPa)	685.34	601.44	483.36	862.18	877.29	619.40	755.69	677.63	502.08
Ultimate Strength (MPa)	703.72	628.63	501.74	896.42	913.25	654.73	785.27	716.32	511.82
Elongation (Pct)	15.72	16.35	17.66	15.76	15.98	17.42	16.23	17.54	18.36

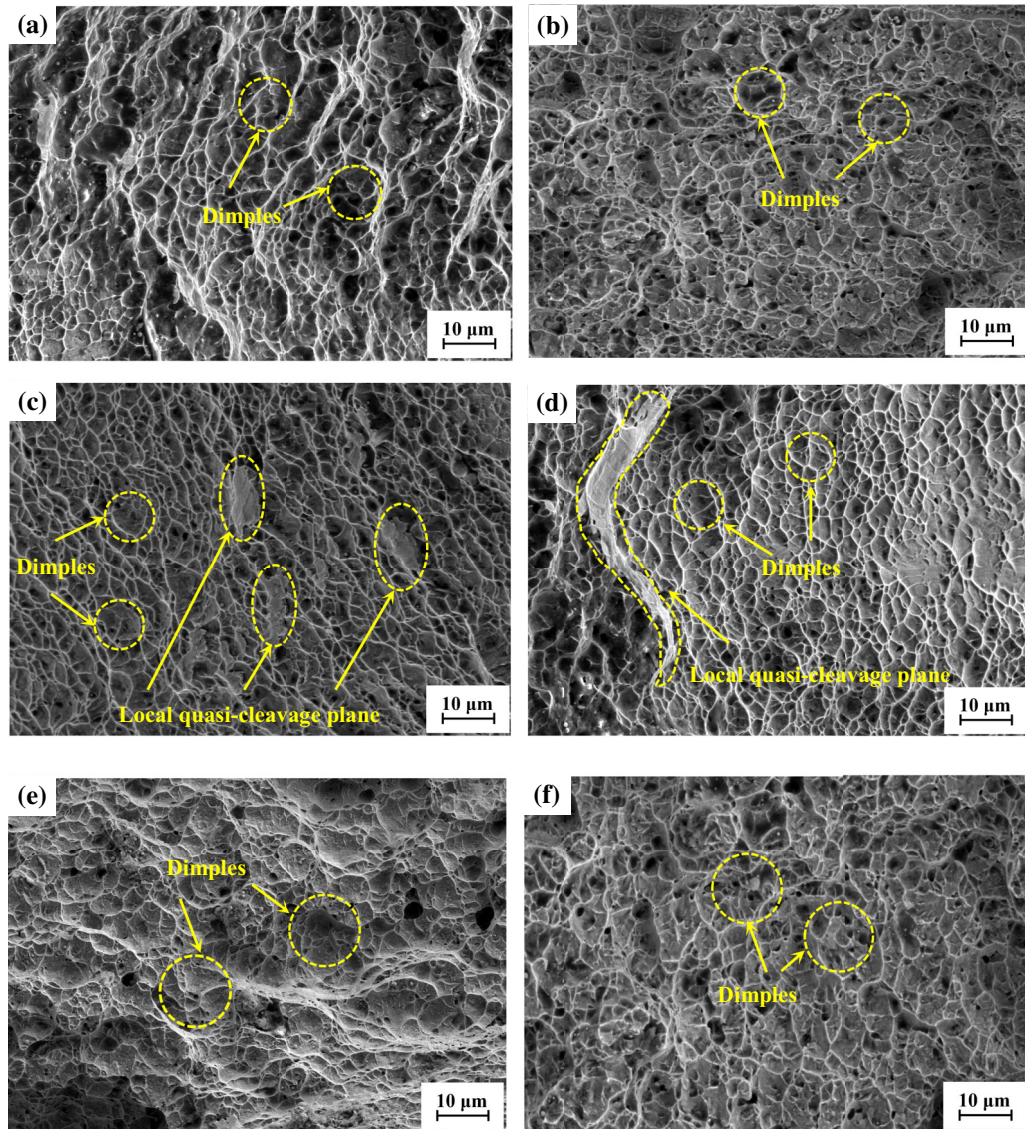


Fig. 11—Tensile fracture morphologies of TC6 samples treated by different treatments: (a) LP + 400 °C, (b) CT-LP + 400 °C, (c) LP + 500 °C, (d) CT-LP + 500 °C, (e) LP + 600 °C, and (f) CT-LP + 600 °C.

high temperature, thus reducing the CRS relaxation and improving the high-temperature mechanical properties.

The instantaneous impact of LP produces abundant dislocation structures on the superficial layer of treated alloys, and simultaneously motivates the rapid movement of dislocations induced by CT. Then, the accumulative high-density dislocation caused by CT-LP is

available to rearrange into dislocation walls, dislocation tangles, as well as dislocation cells, and further divide the original coarse grains into the sub-grains, ultimately evolving into ultra-fine grains. During the CT-LP process, a gradient in plastic deformation with depth from the LPed surface is generated, and as a result, a gradient in residual stress and microstructure is also

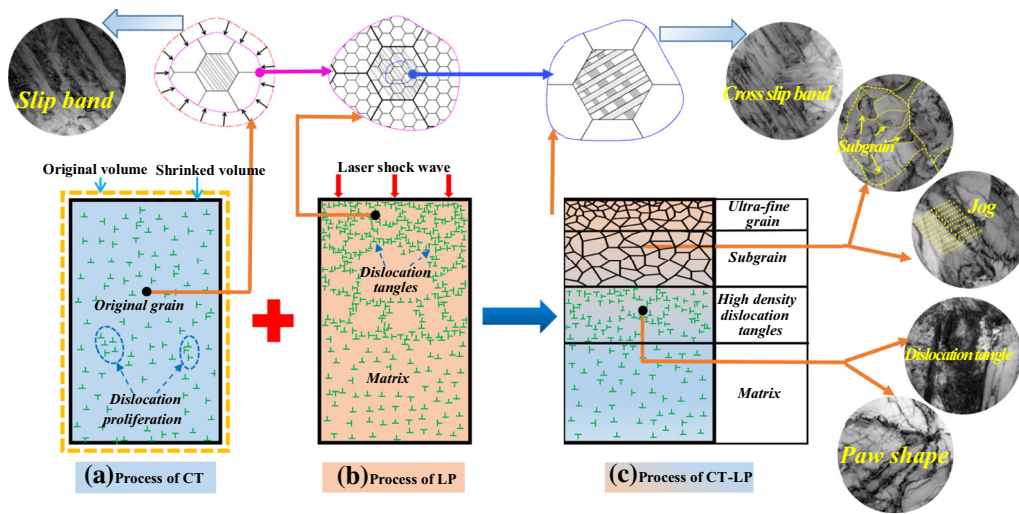


Fig. 12—Schematic illustration of microscopic strengthening mechanism on CT-LPed TC6 titanium alloy: (a) process of CT, (b) process of LP, and (c) process of CT-LPed.

formed.^[44] At the very top surface, intense plastic deformation leads to extreme grain refinement and enormous increase of dislocation density, which causes the formation of dislocation entanglements and slip bands. In the subsurface layer, sub-grain and high-density dislocation tangles are induced. In the interior of material, dislocation structures and slip bands are generated since CT is considered as a “body treatment,” rather than surface treatment, which could effectively enhance the high-temperature strength of the entire material. In addition, ultra-low temperature of CT process can enhance the energy storage of alloys, which significantly increase the number of nucleus during thermal recovery process to obtain a better high-temperature strength.

Actually, microstructures induced by CT-LPed are evolved into different morphologies at high temperature, resulting in a change of mechanical properties and relaxation of residual stress. During the thermal exposure process of CT-LPed samples, the crystal defects such as dislocation tangles, dislocation walls, as well as dislocation cells are partly annihilated; however, the remained dislocation structures still serve as strong obstacles to the migration of grain boundary, thus reducing the grain growth.

It is interesting that typical dislocation jog is observed in the near-surface layer of CT-LPed sample while exposed at 500 °C, as shown in Figure 8. In fact, there exist two kinds of slip process in CT-LP process, including slips induced by volume shrinkage effect during CT process and slips induced by shock pressure during LP, as shown in Figures 8(c) through (e). Since the slip direction generated by LP and CT process is inconsistent, jogs are generated as obstacles for dislocation movement. Especially, unmovable jogs can aggravate dislocation tangle and eventually improve the stability of microstructure at high temperature. A new formed “paw-shaped” structure is found in the near-surface layer of CT-LPed TC6 sample exposed at 600 °C. It is adhered on the grain boundaries and makes the

divisive microstructures with small scale much more stable, as shown in Figure 9. It is noted that even at 600 °C, the new generated dislocation walls are self-tangled. This new structure could be a direct evidence for the strengthening effect of CT-LP process at high temperature.

IV. CONCLUSIONS

The effects of a compound technique combined with cryogenic pre-treatment and laser peening on mechanical properties of TC6 titanium alloy at high temperature were investigated. Strengthening mechanism of the new technique was revealed from both macro- and micro-sides. Some important conclusions can be drawn.

- (1) The relaxation of CRS was ascribed to the thermally activated gliding of dislocations during the thermal recovery process. Relaxation of CRS was increased with the increase of temperature and exposure time. Compared with LP, CRS induced by CT-LP was more stable and still superior. For instance, CRSes of CT-LPed samples were 11.57, 27.54, and 40.52 pct higher than that of LPed samples at 400 °C, 500 °C, and 600 °C for 100 minutes, respectively.
- (2) Both LP and CT-LP induced severe lattice distortion and dislocation proliferation, and thus enhanced the high-temperature mechanical properties. The yield strength of CT-LPed samples was 14.09, 29.46, and 23.37 pct higher than that of the LPed samples at 400 °C, 500 °C, and 600 °C, respectively.
- (3) CT-LP treatment induced more stable strengthening microstructures. A novel “paw-shaped” structure which was adhered on the grain boundaries made the divisive microstructures with small scale much more stable. The jogs generated by the dislocation slipping in multi-direction further

aggravated the dislocation tangle. The cross-slip bands inside the grains inhibited the movement of free dislocations, and contributed to improve the high-temperature mechanical properties.

- (4) Experimental evidence indicates that synergistic effects of ultra-low temperature volumetric shrinkage induced by CT and ultra-high strain rate plastic deformation induced by LP were crucial factors for the strengthening of CT-LP technique at high temperature.

ACKNOWLEDGMENTS

The authors are grateful for the financial support from the National Natural Science Foundation of China (Nos. 51775252, 51405204), China Postdoctoral Science Foundation Funded Project (2018M630526), Six Talent Peaks Project in Jiangsu Province (GDZB-050), Opening Project of Jiangsu Key Laboratory of Large Engineering Equipment Detection and Control (JSKLEDC201503), and Youth Key Teacher Training Project of Jiangsu University (2016016).

REFERENCES

1. E. Ghasemi, A. Zarei-Hanzaki, S. Moemeni, M. Ghambari, and M. Rezaei: *Mater. Sci. Eng. A*, 2016, vol. 654, pp. 264–70.
2. A. Umapathi and S. Swaroop: *Opt. Laser Tech.*, 2018, vol. 100, pp. 309–16.
3. I. Balasundar, K.R. Ravi, and T. Raghu: *Mater. Sci. Eng. A*, 2017, vol. 684, pp. 135–45.
4. A. Schuh, C. Zeller, U. Holzwarth, W. Kachler, G. Wilcke, G. Zeiler, B. Eigenmann, and J. Bigoney: *J. Biomed. Mater. Res. B*, 2007, vol. 81, pp. 330–35.
5. D.Y. Ju, X.M. Fu, S. Na, B. Han, and X.H. Deng: *Adv. Mater. Res.*, 2011, vols. 317–319, pp. 429–35.
6. A.L. Wen, S.W. Wang, R.M. Ren, and X.X. Yan: *Appl. Mech. Mater.*, 2011, vols. 55–57, pp. 1138–41.
7. A. Umapathi and S. Swaroop: *Mater. Charact.*, 2017, vol. 131, pp. 431–39.
8. D. Cellare and M. Reintant: *Mater. Sci. Eng. A*, 2012, vol. 532, pp. 362–72.
9. J. Sheng, J. Zhou, and S. Huang: *Int. J. Adv. Manuf. Tech.*, 2015, vol. 76, pp. 1285–95.
10. B. Ahmad and M.E. Fitzpatrick: *Metall. Mater. Trans. A*, 2017, vol. 48A, pp. 759–70.
11. J.Z. Lu, W.Q. Zhang, and X. Jing: *J. Laser Appl.*, 2017, vol. 29, p. 012007.
12. E. Maawad, Y. Sano, L. Wagner, H.G. Brokmeier, and C. Genzel: *Mater. Sci. Eng. A*, 2012, vol. 536, pp. 82–91.
13. K. Sowmya Joshi, G. Rajyalakshmi, G. Ranjith, S. Kalainathan, and S. Prabhakaran: *Mater. Today*, 2018, vol. 5, pp. 12174–86.
14. J. Sheng, S. Huang, J. Zhou, J. Lu, S. Xu, and H. Zhang: *Opt. Laser Technol.*, 2016, vol. 77, pp. 169–76.
15. R. Bikkelloo, G.H. Farrahi, A. Mehmanparast, and S.M. Mahdavi: *Theor. Appl. Fract. Mech.*, 2020, vol. 105, p. 102429.

16. E. Agyenim-Boateng, S. Huang, J. Sheng, G. Yuan, Z. Wang, J. Zhou, and A. Feng: *Surf. Coat. Technol.*, 2017, vol. 328, pp. 44–53.
17. S. Huang, G. Yuan, J. Sheng, W. Tan, E. Agyenim-Boateng, J. Zhou, and H. Guo: *Int. J. Hydrogen Energy*, 2018, vol. 43, pp. 11263–74.
18. R.K. Nalla, I. Altenberger, U. Noster, G.Y. Liu, B. Scholtes, and R.O. Ritchie: *Mater. Sci. Eng. A*, 2003, vol. 355, pp. 216–30.
19. J. Li, J.Z. Zhou, A.X. Feng, S. Huang, X.K. Meng, Y.H. Sun, and Y.J. Sun: *Mater. Sci. Eng. A*, 2018, vol. 734, pp. 291–98.
20. S. Zhirafar, A. Rezaeian, and M. Pugh: *J. Mater. Process. Tech.*, 2007, vol. 186, pp. 298–03.
21. P.J. Singh, B. Guha, and D.R.G. Achar: *Eng. Fail. Anal.*, 2003, vol. 10, pp. 1–12.
22. M. Araghchi, H. Mansouri, R. Vafaei, and Y. Guo: *Mater. Sci. Eng. A*, 2017, vol. 689, pp. 48–52.
23. J.Z. Zhou, S.Q. Xu, S. Huang, X.K. Meng, J. Sheng, H.F. Zhang, J. Li, Y.H. Sun, and A.B. Emmanuel: *Metals*, 2016, vol. 279, pp. 1–10.
24. C. Ye, S. Suslov, D. Lin, Y.L. Liao, X.L. Fei, and G.J. Cheng: *J. Appl. Phys.*, 2011, vol. 110, pp. 0835041–8.
25. J.Z. Zhou, J. Li, S.Q. Xu, S. Huang, X.K. Meng, J. Sheng, and H.F. Zhang: *Surf. Coat. Tech.*, 2018, vol. 345, pp. 31–39.
26. J.Z. Zhou, J. Li, S. Huang, J. Sheng, X.K. Meng, Q. Sun, Y.H. Sun, G.F. Xu, Y.J. Sun, and H.T. Li: *Mater. Sci. Eng. A*, 2018, vol. 718, pp. 207–15.
27. G.R. Li, J.F. Cheng, H.M. Wang, and C.Q. Li: *J. Alloy Compd.*, 2017, vol. 695, pp. 1930–45.
28. I. Altenberger, R.K. Nalla, Y.J. Sano, L. Wagner, and R.O. Ritchie: *Int. J. Fatigue*, 2012, vol. 44, pp. 292–02.
29. H. Armin and S. Ramin: *Int. J. Adv. Manuf. Tech.*, 2019, vol. 100, pp. 877–93.
30. M. Kattoura, A. Telang, S.R. Mannava, D. Qian, and V.K. Vasudevan: *Mater. Sci. Eng. A*, 2018, vol. 711, pp. 364–77.
31. J.Z. Zhou, Y.H. Han, S. Huang, X.K. Meng, J. Sheng, W.L. Zhu, and S.O. Xu: *Rare Met. Mater. Eng.*, 2016, vol. 45, pp. 1509–14.
32. S.A. Catledge and Y.K. Vohra: *J. Appl. Phys.*, 1999, vol. 86, pp. 698–700.
33. X.L. Wei and X. Ling: *Appl. Surf. Sci.*, 2014, vol. 301, pp. 557–63.
34. J. Yang, H. Jiang, Z.H. Yao, and J.X. Dong: *Mater. Lett.*, 2018, vol. 221, pp. 89–92.
35. K.H. Bae, T.H. Kim, S.R. Lee, H.J. Kim, M.W. Lee, and T.S. Jang: *J. Alloy Compd.*, 2013, vol. 49, pp. 3251–54.
36. C.L. Hale, W.S. Rollings, and M.L. Weaver: *Mater. Sci. Eng. A*, 2001, vol. 300, pp. 153–64.
37. M.D.C. Sobral, P.R. Mei, and H.J. Kestenbach: *Mater. Sci. Eng. A*, 2004, vol. 367, pp. 317–21.
38. D. Hull, J.D. Bacon, and D. Bacon: *Introduction to Dislocations*, 2011, p. 257.
39. A. Pichler, M. Weller, and E. Arzt: *J. Alloy Compd.*, 1994, vols. 211–212, pp. 414–18.
40. B.J.F. Bruet, J. Song, M.C. Boyce, and C. Ortiz: *Nat. Mater.*, 2008, vol. 7, pp. 748–56.
41. C. Ye, A. Telang, A.S. Gill, S. Suslov, Y. Idell, K. Zwiackier, J.M.K. Wiezorek, Z. Zhou, D. Qian, S.R. Mannava, and V.K. Vasudevan: *Mater. Sci. Eng. A*, 2014, vol. 613, pp. 274–88.
42. C. Ye, S. Suslov, B.J. Kim, E.A. Stach, and G.J. Cheng: *Acta Mater.*, 2011, vol. 59, pp. 1014–25.
43. A.I. Dekhtyar, B.N. Mordiyuk, D.G. Savvakina, V.I. Bondarchuk, I.V. Moiseeva, and N.I. Khripta: *Mater. Sci. Eng. A*, 2015, vol. 641, pp. 348–59.
44. M. Kattoura, S.R. Mannava, D. Qian, and V.K. Vasudevan: *Int. J. Fatigue*, 2017, vol. 102, pp. 21–134.

Publisher's Note Springer Nature remains neutral with regard to jurisdictional claims in published maps and institutional affiliations.